Steady-state and transient analysis of the Peskin-Odell-Oster Brownian ratchet model in the limit of large but finite diffusion

Gregory Kozyreff
Optique Nonlinéaire Théorique, Université libre de Bruxelles (U.L.B.), CP 231, Belgium

Jean-Paul Ryckaert
Département de Physique, Université libre de Bruxelles (U.L.B.), CP 223, Belgium

(Received 6 June 2019; published 22 August 2019)

We study the model of growing filament against a wall proposed by Peskin, Odell, and Oster [Biophys. J. **65**, 316 (1993)] using the ratio of chemical to diffusion timescales as a small expansion parameter. A detailed multiple-scale analysis allows us to fully describe the spatiotemporal evolution toward a steady-state distribution for the wall-tip distance, including chemical effects, in very good agreement with numerical simulations. Implications on the quasistatic approximation, where the force on the wall is allowed to vary slowly in time, are discussed. A corrected force-velocity relationship together with explicit expressions of the relevant timescales are provided.

DOI: 10.1103/PhysRevE.100.022132

I. INTRODUCTION

The Brownian Ratchet (BR) model proposed by Peskin, Odell, and Oster [1] serves as the simplest theory of work production by filaments growing against a load in living cells. It describes the stochastic evolution of a rigid straight filament that can polymerize or depolymerize normally against a rigid mobile wall subjected to Brownian motion, with diffusion constant D and a constant force F, see Fig. 1. In this model, the filament grows or shrinks in a stepwise manner by one monomer of size d with respective bulk rates U_0 and W_0. In the supercritical case, defined by $U_0 > W_0$, the filament tip advances with an average velocity $d(U_0 - W_0)$ in the bulk. This growth is slowed down when the filament hits the loaded wall [2]. From that moment onward, the wall Brownian motion becomes limited on one side by the filament tip. In addition, the filament-wall nonoverlapping condition implies that the polymerization process of the filament is only possible if the tip-wall distance is larger than d. Based on these considerations, Peskin *et al.* derived a Fokker-Planck equation leading, after a transient, to a probability distribution $c(x')$ associated to the tip-wall distance. Given $c(x')$, the expected value of the tip velocity is

$$v = d\left[U_0 \frac{\int_d^\infty c(x')dx'}{\int_0^\infty c(x')dx'} - W_0\right]. \tag{1}$$

In the limit where the Brownian motion is characterized by an infinite diffusion coefficient D, $c(x')$ is a simple exponential and the following force-velocity relationship:

$$v = d(U_0 e^{-Fd/k_BT} - W_0) \tag{2}$$

is obtained, where F is the constant force on the wall that is taken positive toward the filament tip. The condition of a vanishing velocity, or "stalling," is therefore reached when $F = F_s = (k_BT/d)\ln(U_0/W_0)$. This result persists in the general case of a finite D and is in agreement with thermodynamical prediction [3]. The interest of the Peskin, Odell, and Oster model is that it simply explains how the free energy released by filament polymerization can be converted into mechanical energy for $0 < F < F_s$. It thus provides a theoretical basis to understand such chemomechanical processes in biological cells. The purpose of this paper is to present new analytical results on this model when D is large but finite.

The above theory obviously rests on a series of approximations, which need to be appreciated when the BR model is used to interpret an *in vivo* or *in vitro* experimental result involving growing filaments against a loaded wall. In short, the most relevant approximations [2,4] are as follows: the filaments are usually semiflexible, the self-assembly kinetics may involve more chemical steps than a simple monomer interconversion between a free and a bounded state [e.g., as the hydrolysis of ATP(GTP)-protein monomeric complexes], the (de)polymerization rates which are treated as constant could be varying as the tip approaches the obstacle (e.g., free monomer density inhomogeneities would affect the first order polymerization rate). Moreover, the hard flat wall describing the loaded obstacle neglects possible surface fluctuations if the mobile obstacle is a patch of the cell membrane [5–7]. Theoretically, it is important to stress that with the above simplifications, the BR model leads to a relatively simple stochastic problem when the load force is considered as constant [1]. Indeed, it then leads asymptotically to a time-independent tip-wall distance distribution and a stationary velocity. To assess the experimental relevance of this model, one should pay special attention to two modeling assumptions, namely the choice of a constant force and the rigid filament approximation. The hypothesis of a constant force is met in some *in vitro* experiments [8] but also in specific *in vivo* dynamical situations like the growth or shrinking of filopedia protrusions [4,9–11]. In this situation, a bundle of parallel actin filaments, emerging from the cytoskeleton, develop fingerlike membrane-actin structures growing as long as the

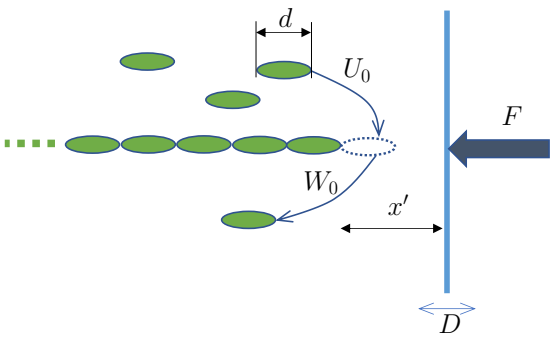

FIG. 1. Schematic representation of the Brownian ratchet. A polymer filament grows by the addition of monomers of size d at its tip with a rate U_0, under the condition that a gap $x' > d$ is available for this process. Meanwhile, the tip suffers detachments with rate W_0 and the wall, subjected to a force F, moves with a one-dimensional Brownian motion with diffusion coefficient D.

polymerizing force overcomes the membrane resisting force [5]. For strong deformations by a bundle of a few filaments, as the membrane develops a tubelike protuberance, the resisting force is essentially constant $F \approx \pi(8\kappa\sigma)^{1/2}$ where σ is the cell membrane tension and κ its bending rigidity coefficient [12]. Hence, the BR model in its elementary form with a hard wall modeling the tip-membrane contacts and a constant load force was proposed, in its multifilaments extension, as a basic model to describe filopodium dynamics [5]. Moreover, *in vitro* experiments which probe actin bundle growth against a load using an actin bundle glued on a colloid growing against another colloid or against a solid wall in a water solution of monomeric G-actin have been interpreted with BR models [8,13,14]. Regarding flexibility, bending effect are known to be small for single filaments [15–17] as long as the length L of the working filament satisfies $L < L_\star = [l_p d/\ln(U_0/W_0)]^{1/2}$ where l_p is the persistence length of the filament [18]. For $L > L_\star$, the filament undergoes a "pushing catastrophe" whereby large bending fluctuations allow it to escape laterally, thus decoupling further polymerization from the wall Brownian motion [16]. For actin filament with $l_p = 15\ \mu\text{m} = 5370$ d, one estimates that $L_\star \approx 70$–75 d. Hence, despite its simplicity, the BR model by Peskin *et al.* is still relevant as long as $L < L_\star$.

The single filament BR model contains one obvious natural length scale d but two intrinsic timescales: the diffusion timescale d^2/D and the chemical timescale U_0^{-1}. We denote their ratio as

$$\epsilon = \frac{U_0 d^2}{D}. \tag{3}$$

Usually, it is assumed that $\epsilon \ll 1$ and, indeed, Eq. (2) holds in the limit $\epsilon \to 0$. The purpose of this paper is to provide new analytical results for finite ϵ. Indeed, this parameter appears to be quite variable from one experiment to another. Keeping the monomer length d fixed, ϵ can vary either through the monomer attachment rate U_0 or through the diffusion constant D of the obstacle. U_0 is proportional to the monomer concentration. This concentration can be monitored by the supercriticality parameter U_0/W_0, since W_0 is concentration independent. Next, the diffusion coefficient D of the obstacle depends on its size and of the surrounding fluid viscosity, the latter being significantly larger in a biological cell than in pure water. In *in vitro* experiments [8,13] dealing with micron-size colloids that squeeze actin bundles in water solution at moderate supercriticality, $U_0/W_0 \approx 3$, one estimates that ϵ is on the order of 10^{-4} [14]. However, ϵ is closer to unity when actin polymerization pushes against larger colloids or bacteria. Considering the more viscous nature of the cellular fluid and the much higher supercriticality, one has $10 < U_0/W_0 < 100$, *in vivo* [19,20]. When the simple BR model is used to represent filopedium growth, it was argued that effective values of D for a membrane patch *in vivo* could be found in as large a range as $1\ \text{nm}^2\ \text{s}^{-1} < D < 10^7\ \text{nm}^2\ \text{s}^{-1}$ [5]. Assuming a plausible value $U_0 = 20\ \text{s}^{-1}$, this leads to quite an uncertainty: $10^{-5} < \epsilon < 200$. Taking membrane deformation into account, either through softer potentials [16,20] or using discretized membrane patches [5,6], the definition of D is not so straightforward, but ϵ can still be defined as the ratio of the relaxation time of the local membrane configuration to the chemical timescale. When the membrane is flexible, the filament growth velocity generally increases [5] but in a way that depends on ϵ [16,20]. On the other hand, recent stochastic filopedium models [7,21] assume very fast membrane relaxation times in the μs to ms range. In such a situation, corresponding to $\epsilon \to 0$, the membrane is always in equilibrium relative to the tip position and simply redistributes the total force on the tips.

Most of the established knowledge of the BR model, as for instance expression (2), is restricted to the limit $\epsilon \to 0$, that is, when the wall instantaneously reaches equilibrium between successive gain or loss of monomer by the filament. For multifilament extensions of the BR model, the stationary velocity also depends on the number of filaments and on the filament seeds longitudinal distribution. Quite generally, the $\epsilon = 0$ case remains much easier to treat theoretically, given the effective timescale separation. Analytical results are known for the two-filament case at $\epsilon = 0$ in the unstaggered seed disposition [22]. In the same limit, approximate mean-field approaches have been developed for many filaments BR models, both for unstaggered [22] and for staggered [8] seed arrangements.

For general ϵ, Peskin *et al.* were able to solve their model only if $W_0 = 0$. For general value of W_0 and finite ϵ, no analytical result are documented to our knowledge. Stochastic dynamics approaches for multifilament cases with different seed dispositions have shown a systematic and large slowing down of the wall stationary velocity as ϵ increases and approaches unity [19].

Finite-ϵ values cause correlations between successive jumps; this is a clear challenge compared to the case $\epsilon = 0$, where the wall reaches its equilibrium position between successive independent polymerization-depolymerization events. From the literature survey above, it appears that only limited information is known about the crucial influence of a finite ϵ on the BR dynamics. Hence, in the present work, we propose a systematic study of the BR model for small but nonzero ϵ. In steady state, we find significant deviation from the usually expected exponential behavior of $c(x')$ in the immediate vicinity of the wall; away from the wall, the rate of the exponential is perturbed by ϵ. A perturbation framework is presented which allows a high-precision evaluation of ϵ-related effects and

which appears to be quantitatively accurate in the entire range $\epsilon \in [0, 1]$.

In addition, using the method of multiple scales, we analytically determine the time evolution of the probability distribution toward its steady profile. This yields the timescale on which $O(\epsilon)$ corrections affect the distribution. Moreover, we compute the temporal evolution of v, which allows us to establish the conditions of quasistatic approximation, that is, when a time-dependent F varies sufficiently slowly for the system to sample in succession quasistationary states.

II. DIFFUSION MODEL

The Peskin-Odell-Oster model [1] is a Fokker-Planck equation for the time-dependent probability distribution $c(x', t')$ associated to the distance x' between the wall and the tip of the growing filament:

$$\frac{\partial c}{\partial t'} = D\frac{\partial^2 c}{\partial x'^2} + \frac{FD}{k_B T}\frac{\partial c}{\partial x'} + U_0 c(x'+d, t') - W_0 c(x', t') + H(x'-d)[W_0 c(x'-d, t') - U_0 c(x', t')] \tag{4}$$

with boundary conditions

$$D\frac{\partial c}{\partial x'} + \frac{FD}{kT}c = 0, \quad x' = 0, \tag{5}$$

$$c \to 0, \quad x' \to \infty, \tag{6}$$

and where $H(x')$ is the Heaviside function. The chemical terms in Eq. (4) make it a differential-difference equation and, hence, generally hard to solve. Fortunately, in situations of interest, these terms are expected to be sufficiently small to be treated as perturbation.

III. MULTIPLE-SCALE ANALYSIS

As it tends to zero, the factor ϵ infinitely separates the chemical and diffusion timescales. In addition, two asymptotically distinct spatial scales arise, d and D/dU_0, also in a ratio $\epsilon : 1$ one to the other. The second length scale may be intuited as follows. Given the length d and the time d^2/D, one deduces a drift speed D/d of a diffusing particle that is "ratcheted" at d intervals [1]; the length D/dU_0 then corresponds to the distance covered at this drift speed after a time U_0^{-1}. In the frame of multiple-scale analysis, we thus define

$$t = t'D/d^2, \quad \tau = U_0 t' = \epsilon t, \tag{7}$$

$$x = x'/d, \quad X = dU_0 x'/D = \epsilon x, \tag{8}$$

and formally allow c to depend separately on each of these space and timescales:

$$c = c(x, X, t, \tau). \tag{9}$$

In this way,

$$\frac{\partial c}{\partial t'} \to \frac{D}{d^2}\left(\frac{\partial c}{\partial t} + \epsilon\frac{\partial c}{\partial \tau}\right), \tag{10}$$

$$\frac{\partial c}{\partial x'} \to \frac{1}{d}\left(\frac{\partial c}{\partial x} + \epsilon\frac{\partial c}{\partial X}\right), \tag{11}$$

$$\frac{\partial^2 c}{\partial x'^2} \to \frac{1}{d^2}\left(\frac{\partial^2 c}{\partial x^2} + 2\epsilon\frac{\partial^2 c}{\partial x \partial X} + \epsilon^2\frac{\partial^2 c}{\partial X^2}\right). \tag{12}$$

This transforms Eq. (4) into

$$c_t + \epsilon c_\tau = c_{xx} + \omega c_x + \epsilon\{2c_{xX} + \omega c_X + c(x+1, t) - \beta c(x, t) + H(x-1)[\beta c(x-1, t) - c(x, t)]\} + \epsilon^2 c_{XX}, \tag{13}$$

where we have used subscripts to denote differentiation and where we have introduced the dimensionless force and monomer detachment rate,

$$\omega = \frac{Fd}{k_B T}, \quad \beta = \frac{W_0}{U_0}. \tag{14}$$

The boundary condition is also altered and now reads

$$c_x + \epsilon c_X + \omega c = 0, \quad \text{at } x = 0. \tag{15}$$

IV. SHORT-TIME TRANSIENT

Over short timescales, that is, $t = O(1)$ and $\tau \ll 1$, the $O(\epsilon)$ terms of Eq. (13) do not affect the solution to leading order and the dynamics is purely diffusive. Expanding c as

$$c \sim c_0 + \epsilon c_1 + \ldots, \tag{16}$$

we find, at leading order, that

$$c_{0,t} = c_{0,xx} + \omega c_{0,x}, \tag{17}$$

with $c_{0,x} + \omega c_0$ on $x = 0$. Let us assume the initial condition

$$c_0 = \delta(x - x_0), \quad t = 0. \tag{18}$$

The solution of this problem is (see Appendix A)

$$c_0 = \frac{e^{-(x-x_0+\omega t)^2/4t}}{2\sqrt{\pi t}}(1 + e^{-x x_0/t}) + \omega e^{-\omega x}\frac{1}{2}\mathrm{erfc}\left(\frac{x + x_0 - \omega t}{2\sqrt{t}}\right). \tag{19}$$

As time progresses, with $(x_0 + x)/\omega \ll t \ll 1/\epsilon$, one has

$$c_0 \to \omega e^{-\omega x}, \tag{20}$$

an expected result if one considers Eq. (17) in steady state.

Let us now assume that, initially, the tip of the polymer touches the wall with absolute certainty: $x_0 = 0$. Then, from Eq. (19) for a given x, the duration of the fast transient is on the order of x/ω and is therefore position dependent. For the exponential dependence in Eq. (20) to fully reveal itself, it must be attained for values of x at least as large as a few times $1/\omega$. Therefore, the duration of the fast transient can be estimated to be on the order of

$$t_s = 1/\omega^2. \tag{21}$$

Dimensionally, this is

$$t_s' = \left(F^2 D/k_B^2 T^2\right)^{-1}. \tag{22}$$

The above analysis allows us to enunciate a criterion for quasistatic approximation in the case of a time-dependent force. If F is a function of time, then one may assume that $c(x, t) \simeq \omega(t)\exp[-\omega(t)x] + O(\epsilon)$ with $\omega(t) = F(t)d/k_B T$ provided that F varies slowly over a time t_s. The quasistatic approximation, if satisfied, may greatly simplify the analysis

of generalizations of the Peskin model where F is not constant. Indeed, it was recently found to be applicable when F is a position-dependent force of the harmonic form, as in an optical trap [14]. There, even though F was not constant in time, Eq. (2) was found to be well verified along most of the trajectory (with some modifications accounting for a bundle of fibres instead of a single one.) Note that t_s diverges as $\omega \to 0$, leading to a breakdown of quasistatic approximation for small forces.

It is instructive to rewrite the quantity in parenthesis in Eq. (22) as

$$\frac{F^2 D}{k_B^2 T^2} = \frac{F\mathcal{V}}{k_B T}, \tag{23}$$

where $\mathcal{V} = FD/(k_B T)$ is the drift velocity of the wall in the absence of the polymer. It thus represents the rate at which the force F dissipates an energy $k_B T$ in the absence of the polymer. The condition of quasistatic evolution is therefore that F, with its point of application moving at speed $\mathcal{V}$, must be able to dissipate an energy $k_B T$ before it changes appreciably.

V. LONG-TIME TRANSIENT

Expression (20) only gives the outcome of the initial transient before chemical effects significantly affect the dynamics. The general steady-state solution of Eq. (17) is $C\omega e^{-\omega x}$, where C is independent of x and t and is trivially equal to 1 here. However, Eq. (17) only faithfully represents Eq. (13) for a brief period of time. In reality, because of the slowly acting chemistry, C is not a constant but rather a function that varies slowly with space and time: $C = C_0(X, \tau)$. This statement is compatible with Eq. (17) if $\lim_{\tau\to 0} C_0(X, \tau) = 1$. More generally, after fast temporal processes have died out, we assume that

$$c \sim C_0(X, \tau)\omega e^{-\omega x} + \epsilon c_1(x, X, \tau) + O(\epsilon^2). \tag{24}$$

Substituting this expansion in Eq. (13), we obtain

$$c_{1,xx} + \omega c_{1,x} = \omega e^{-\omega x}\{C_{0,\tau} + \omega C_{0,X} - [e^{-\omega} - \beta + H(x-1)(\beta e^{\omega} - 1)]C_0\}. \tag{25}$$

For $x > 1$, it is easy to find that

$$c_1 = C_1(X, \tau)\omega e^{-\omega x} - [C_{0,\tau} + \omega C_{0,X} + (e^{-\omega} - \beta)(e^{\omega} - 1)C_0]x e^{\omega x}, \tag{26}$$

where $C_1(X, \tau)$ is an arbitrary function of X and τ only. Above, the $xe^{\omega x}$ contribution is unacceptable because it breaks the assumption that $\epsilon c_1 \ll c_0$ as soon as $x = O(1/\epsilon)$. The exclusion of this possibility leads to the *solvability condition*,

$$C_{0,\tau} + \omega C_{0,X} = -(e^{-\omega} - \beta)(e^{\omega} - 1)C_0, \tag{27}$$

which determines the evolution of $C_0(X, \tau)$ over long spatial and temporal scales (see the next section). Therefore, for $x > 1$, Eq. (25) yields, simply,

$$c_1 = C_1(X, \tau)\omega e^{-\omega x}, \tag{28}$$

while, in the range $0 < x < 1$, we have to solve

$$c_{1,xx} + \omega c_{1,x} = -\omega e^{-\omega x}(e^{-\omega} - \beta)e^{\omega} C_0(X, \tau). \tag{29}$$

Imposing continuity of c_1 and $c_{1,x}$ at $x = 1$, this gives

$$c_1 = \left[\frac{1 - e^{\omega(x-1)}}{\omega} + x - 1\right](1 - \beta e^{\omega})C_0(X, \tau)e^{-\omega x} + C_1(X, \tau)\omega e^{-\omega x}. \tag{30}$$

Combining the information gathered so far, we find that

$$c \sim \omega e^{-\omega x}\left\{C_0(X, \tau) + \epsilon C_1(X, \tau) - \frac{\epsilon}{\omega}H(1-x) \times \left[\frac{e^{\omega(x-1)} - 1}{\omega} + 1 - x\right](1 - \beta e^{\omega})C_0(X, \tau)\right\}. \tag{31}$$

A complete description of c including all $O(\epsilon)$ terms above requires one to determine the function $C_1(X, \tau)$. This function is again determined by a solvability condition, to be found at $O(\epsilon^2)$ of the calculation. In the Appendix, we show that, in fact, C_1 is an arbitrary multiple of C_0. Hence, the presence of C_1 only amounts to change C_0 into $(1 + \epsilon\ \text{const})C_0$, i.e., c into $(1 + \epsilon\ \text{const})c$. Such a factor has no influence when using c to compute observable quantities; see, for instance, Eq. (1). Therefore, we may simply omit C_1 it and write

$$c \sim \omega e^{-\omega x} C_0(X, \tau)\left\{1 - \epsilon\frac{1 - \beta e^{\omega}}{\omega} \times \left[\frac{e^{\omega(x-1)} - 1}{\omega} + 1 - x\right]H(1-x)\right\}. \tag{32}$$

VI. DETERMINATION OF $C_0(X, \tau)$

In the previous section, we have derived the evolution equation

$$C_{0,\tau} + \omega C_{0,X} = -(e^{-\omega} - \beta)(e^{\omega} - 1)C_0, \tag{33}$$

which is a first-order partial differential equation involving derivatives with respect to the slow variables X and τ. The domain of definition of C_0 is the quarter-plane where both X and τ are positive. Before we can solve Eq. (33), we must specify C_0 on the semilines $\tau = 0$ and $X = 0$. On the one hand, the initial condition follows from Sec. IV:

$$C_0(X, 0) = 1. \tag{34}$$

On the other hand, in order to determine $C_0(0, \tau)$, we consider the boundary condition (15). Evaluating it with the aid of Eq. (32), we find

$$\omega C_{0,X}(0, T) = (1 - \beta e^{\omega})(1 - e^{-\omega})C_0(0, T). \tag{35}$$

Inserting this expression into Eq. (33) with $X = 0$, we find that

$$C_{0,\tau}(0, \tau) = 0. \tag{36}$$

Hence, we have, simply,

$$C_0(0, \tau) = 1 \tag{37}$$

for all τ.

A. Resolution of the PDE

Equation (33) can be completely solved by the method of characteristics [23]. The idea is to find a curve in the (X, τ) plane along which the partial differential equation becomes

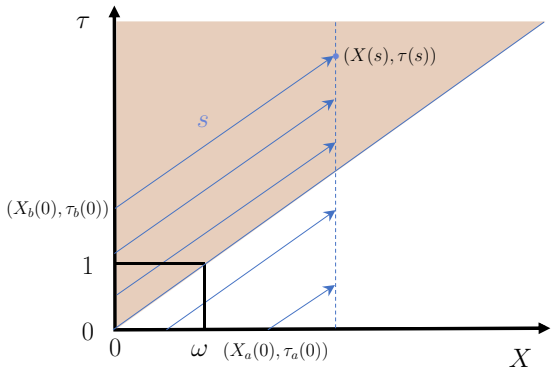

FIG. 2. Schematic drawing of the characteristics of Eq. (33). The evolution of the solution takes place along the blue characteristic curves with parameter s. For small τ, a given point X is in the zone of influence of the initial data on the semiaxis $\tau = 0$, such as the point $(X_a(0), \tau_a(0))$. Later, in the shaded region, the point X is on a characteristic that emanates from a point $(X_b(0), \tau_b(0))$ the semiaxis $X = 0$. From that moment onward, the Cauchy data on that semiaxis are constant and the length s along the characteristic that reaches X is also constant. Hence $C_0(X, \tau)$ is independent of τ in the shaded area.

an ordinary one. Such a curve generally exists: It is the characteristic curve. Let this curve be parameterized as

$$X = X(s), \quad \tau = \tau(s). \tag{38}$$

Along this curve, $C_0 = C_0(s)$ with

$$\frac{dC_0}{ds} = C_{0,\tau}\frac{d\tau}{ds} + C_{0,X}\frac{dX}{ds}. \tag{39}$$

Combining this piece of information with (33), we find $d\tau/ds = 1$, $dX/ds = \omega$, and

$$\frac{dC_0}{ds} = -(e^{-\omega} - \beta)(e^{\omega} - 1)C_0(s). \tag{40}$$

This trivially yields

$$X(s) = X(0) + \omega s, \tag{41}$$

$$\tau(s) = \tau(0) + s, \tag{42}$$

$$C_0(s) = C_0(0)e^{-(e^{-\omega}-\beta)(e^{\omega}-1)s}. \tag{43}$$

At the start of the characteristic curve, $s = 0$, we have the initial conditions $X = X(0)$, $\tau = \tau(0)$, and $C = C(0)$. In the present situation, $C(0) = 1$ for all characteristics curves.

In the region $0 < \tau < X/\omega$, the characteristic emanates from $\tau = 0$, see Fig. 2. Hence,

$$\tau = s, \quad X(0) = X - \omega\tau, \quad C_0 = e^{-(e^{-\omega}-\beta)(e^{\omega}-1)\tau}. \tag{44}$$

At later times, when $\tau > X/\omega$, they stem from $X = 0$. We thus have

$$s = \frac{X}{\omega}, \quad \tau = \tau(0) + \frac{X}{\omega}, \quad C_0 = e^{-(e^{-\omega}-\beta)(e^{\omega}-1)X/\omega}. \tag{45}$$

Combining Eqs. (44) and (45), we obtain

$$C_0(X, \tau) = e^{-(e^{-\omega}-\beta)(e^{\omega}-1)\min(\tau, X/\omega)}. \tag{46}$$

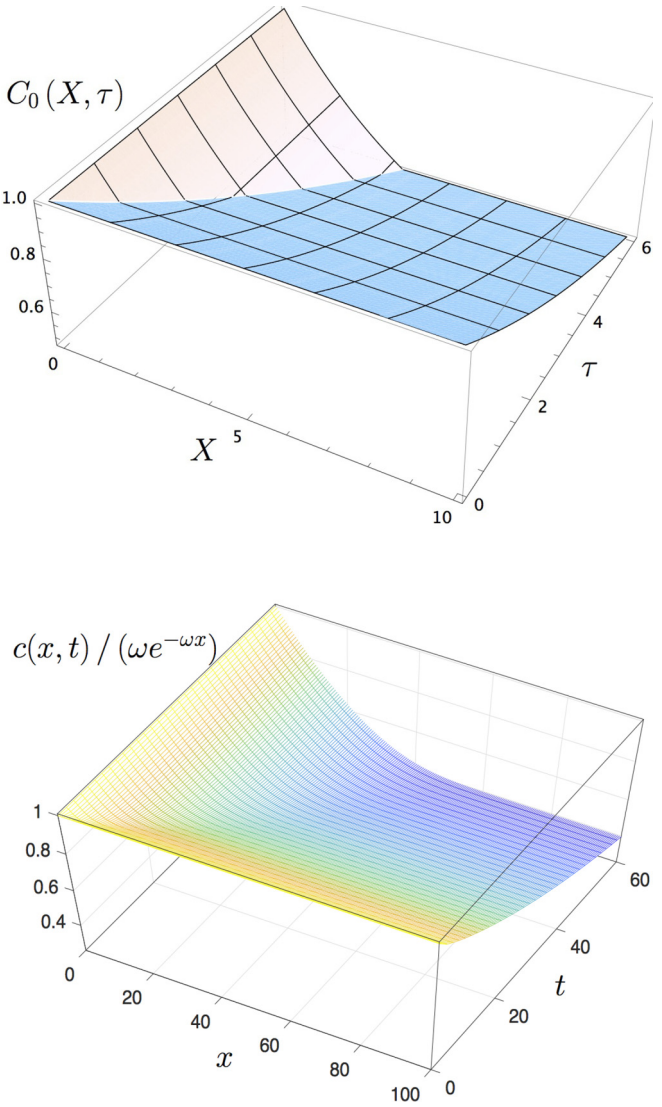

FIG. 3. Top: Evolution of the slowly varying amplitude $C_0(X, \tau)$ for $\omega = 0.6$ and $\beta = 0.4$ according to Eq. (46). Bottom: $\omega^{-1}c(x, t)e^{\omega x}$ from direct numerical simulation of Eq. (4) with the same parameters and $\epsilon = 0.1$. The initial condition is given by Eq. (20). A MATLAB code to numerically simulate the Fokker-Planck equation is provided as the Supplemental Material [24] of this article.

This is illustrated in Fig. 3 and compared with $c(x, t)/(\omega e^{-\omega x})$ as obtained by direct numerical integration of Eq. (4), showing very good agreement.

Considering Eqs. (32) and (46), we have thus established that, after a transient, when $\tau > X/\omega$,

$$c \sim \omega e^{-\mu x}\left\{1 - \epsilon\frac{1-\beta e^{\omega}}{\omega} \times \left[\frac{e^{\omega(x-1)}-1}{\omega} + 1 - x\right]H(1-x)\right\}, \tag{47}$$

where

$$\mu \sim \omega + \frac{\epsilon}{\omega}(1-\beta e^{\omega})(1-e^{-\omega}) + O(\epsilon^2). \tag{48}$$

Equivalently, at this order of approximation, we may write

$$c \sim \mu e^{-\mu x}\left\{1-\epsilon\frac{1-\beta e^{\mu}}{\mu} \times\left[\frac{e^{\mu(x-1)}-1}{\mu}+1-x\right]H(1-x)\right\}. \tag{49}$$

Equation (46) implies that the duration of the transient is given by

$$\tau \sim X/\omega \leftrightarrow t \sim x/\omega. \tag{50}$$

In the unscaled coordinate, this is

$$t' \sim \frac{x'}{FD/k_BT}. \tag{51}$$

The denominator above is simply the drift velocity of the obstacle in response to the force F. The time required for $O(\epsilon)$ effects to reach steady state is equal to the duration of the transient in the $X = O(1)$ region, which is $x' = O(d/\epsilon)$. An estimate of this time is

$$t'_\epsilon = \frac{d}{\epsilon FD/k_BT} = \frac{U_0^{-1}}{Fd/k_BT}. \tag{52}$$

VII. STEADY STATE

After having established the transient evolution over short and long timescales, we now describe the steady-state solution in more detail. We first note that in the limit $x \to \infty$, Eq. (4) has the exponential solution $c \sim e^{-\mu x}$ with

$$\mu(\mu-\omega)-\epsilon(e^{-\mu}-\beta)(e^{\mu}-1)=0. \tag{53}$$

This is consistent to $O(\epsilon)$ with Eq. (48) derived by the multiple-scale analysis. By expressing c as

$$c = \mu e^{-\mu x}\times h(x) \tag{54}$$

and making use of Eq. (53), we transform the original equation into

$$h_{xx}-\mu h_x = \epsilon\{\nu(h_x-\mu h)+\beta h - e^{-\mu}h(x+1) + H(x-1)[h-\beta e^{\mu}h(x-1)]\}, \tag{55}$$

with

$$h_x = \epsilon\nu h, \quad x=0 \tag{56}$$

$$h \to \text{const}, \quad x\to\infty, \tag{57}$$

where we have introduced the shorthand notation

$$\nu = \frac{(e^{-\mu}-\beta)(e^{\mu}-1)}{\mu}. \tag{58}$$

This puts the differential problem in a convenient form for further asymptotic analysis in the small-ϵ limit. Let us expand h as

$$h(x) \sim \sum_{n\geqslant 0}\epsilon^n h_n(x). \tag{59}$$

Collecting terms of equal power of ϵ in Eq. (55), we first obtain

$$h_0(x) = 1. \tag{60}$$

Using this solution, we find at next order that

$$h_{1,xx}-\mu h_{1,x} = -(1-\beta e^{\mu})H(1-x), \tag{61}$$

with

$$h_{1,x} = \nu, \quad x=0 \tag{62}$$

$$h_1 \to 0, \quad x\to\infty. \tag{63}$$

The solution is

$$h_1 = -\frac{1-\beta e^{\mu}}{\mu}\left[\frac{e^{\mu(x-1)}-1}{\mu}+1-x\right]H(1-x). \tag{64}$$

Hence, in terms of $c(x)$ the solution is, up to $O(\epsilon)$

$$c \sim \mu e^{-\mu x}\left\{1-\epsilon\frac{1-\beta e^{\mu}}{\mu} \times\left[\frac{e^{\mu(x-1)}-1}{\mu}+1-x\right]H(1-x)\right\}, \tag{65}$$

in full $O(\epsilon)$ agreement with Eq. (49), derived by the method of multiple scales. At second order, we have

$$h_{2,xx}-\mu h_{2,x} = \begin{cases} f_{21}, & 0<x<1,\\ f_{22}, & 1<x<2,\\ 0, & 2<x,\end{cases} \tag{66}$$

where f_{21} and f_{22} are given by

$$f_{2,1}(x) = -\frac{1}{\mu^2}(\beta e^{\mu}-1)\{-2\beta e^{\mu(x-1)}+\beta e^{\mu}[\mu(2x-3)+1] + \beta+\mu(e^{-\mu}-1)(x-1)\} \tag{67}$$

and

$$f_{2,2}(x) = \frac{\beta e^{\mu}}{\mu^2}(\beta e^{\mu}-1)[\mu(x-2)-e^{\mu(x-2)}+1]. \tag{68}$$

The solution is

$$h_2 = h_{2,1}H(1-x)+h_{2,2}H(2-x) \tag{69}$$

with

$$h_{2,1} = \frac{(\beta e^{\mu}-1)}{2\mu^4}\{2\beta e^{\mu}[\mu^2(x^2-3x+2)+\mu(3x-4)+3] + (\beta+2)^2-5-(\mu x-\mu+1-\beta)^2 + 2\beta(\mu-3)e^{\mu x}+e^{\mu(x-1)}[4\beta\mu(x-1)-6\beta+2] + e^{-\mu}[(\mu x-\mu+1)^2+1]-2e^{\mu(x-2)}\} \tag{70}$$

and

$$h_{2,2} = -\frac{\beta e^{\mu}(\beta e^{\mu}-1)\left\{\mu^2(x-2)^2+4\mu(x-2)+2e^{\mu(x-2)}[\mu(x-2)-3]+6\right\}}{2\mu^4}. \tag{71}$$

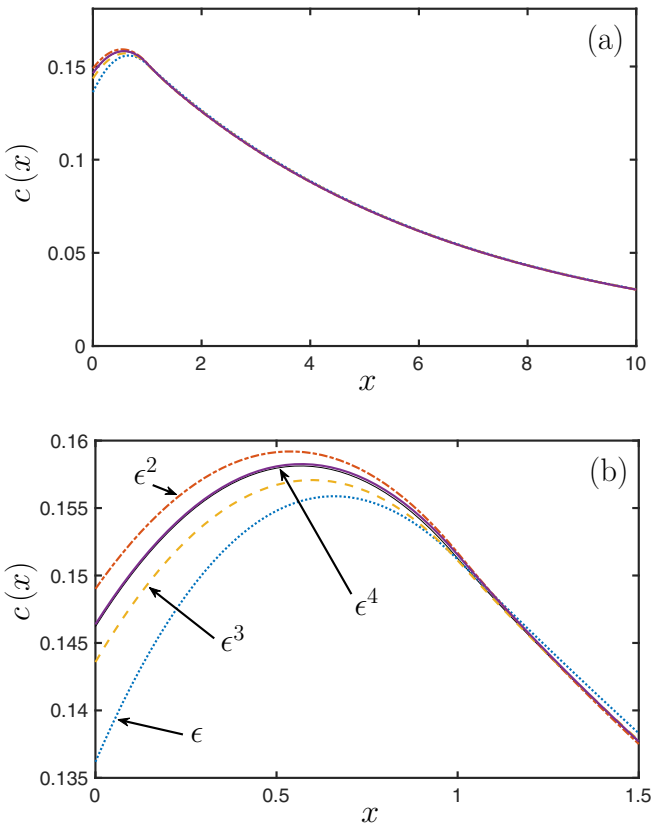

FIG. 4. (a) Comparison of the numerical solution of Eq. (4) with asymptotic approximations of increasing orders of accuracy. Parameters used: $\epsilon = 1$, $\omega = -0.3$, $\beta = 0.4$, corresponding to $\mu = 0.1781$. (b) Blow-up in the range $0 < x < 1.5$. The arrows indicate the order of the approximations. The solution including $O(\epsilon^4)$ terms is undistinguishable from the numerical solution. Both the numerical and the approximate solutions are normalized so that $\int_0^\infty c(x)dx = 1$.

(These expressions are regular as $\mu \to 0$, despite the μ^{-4} factor.) There is no conceptual difficulty to progress to higher orders, but the expressions rapidly become involved and a symbolic software becomes necessary. What transpires from above is that, at order ϵ^n of the calculation, one may decompose the solution as

$$h_n = \sum_{k=1}^{n} h_{n,k} H(k - x). \tag{72}$$

This is useful to implement an automated resolution to arbitrary order. A MATHEMATICA code is provided as Supplemental Material [24]. In order to deal with values of ϵ as large as $\epsilon = 1$, we found that the above solution with $O(\epsilon^2)$ contributions already gives very good accuracy and that including terms up to $O(\epsilon^4)$ yields an approximation that is almost undistinguishable from the numerical one. We illustrate this claim by the comparison in Fig. 4, done with $\epsilon = 1$, $\beta = 0.4$ and a dimensionless force $\omega = -0.3$, corresponding to pulling the obstacle rather than pushing it (negative values of ω are forbidden if $\epsilon = 0$). For smaller ϵ, the agreement further improves rapidly. Note the markedly nonexponential behavior of $c(x)$ near $x = 0$; this results from the polymerization inhibition caused by the wall.

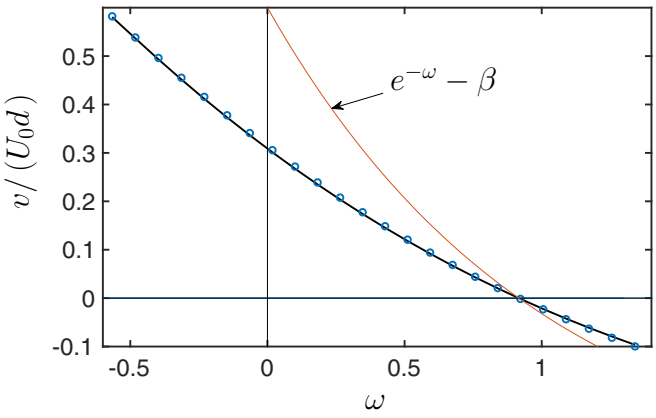

FIG. 5. Numerically computed (full line) and analytically computed (circles) force-velocity relationship with $\epsilon = 1$ and $\beta = 0.4$ using Eqs. (75) and (76). The orange curve shows Eq. (2), known for $\epsilon = 0$. Note that a positive power of transduction Fv of chemical energy into work against the load is only possible where both ω and v are positive.

Not shown in Fig. 4 is the perfect agreement between $c(x)$ as computed by direct numerical integration of the Fokker-Planck Eq. (4) and the distribution obtained from a large number of trajectories using the space discretization of the stochastic dynamics algorithm of Wang *et al.* [14,25]. Note, however, that it is much faster in the present case to solve Eq. (4) than to gather the necessary statistics from the discrete system.

VIII. DISCUSSION

A. Corrected force-velocity relation

At stationarity, the wall velocity coincides with the polymer tip velocity, given by Eq. (1). Using Eq. (65), we obtain

$$\int_0^\infty c dx \sim 1 - \frac{\epsilon}{\mu^2}[\mu - 2 + (\mu + 2)e^{-\mu}](1 - \beta e^{\mu}) + O(\epsilon^2) \tag{73}$$

and

$$\int_1^\infty c dx \sim e^{-\mu} + O(\epsilon^2). \tag{74}$$

Thus, the force-velocity formula becomes

$$v/(U_0 d) \sim (e^{-\mu} - \beta)\left\{1 + \frac{\epsilon}{\mu^2}[\mu - 2 + (2 + \mu)e^{-\mu}]\right\}, \tag{75}$$

$$\omega = \mu - \epsilon(e^{-\mu} - \beta)\frac{e^{\mu} - 1}{\mu}. \tag{76}$$

Given ϵ and β, the above expressions yield a simple and explicit parametrization $(\omega(\mu), v(\mu))$ of the force-velocity relationship as a function of the rate of exponential decay μ of the distribution $c(x)$. This representation compares very favorably with the result of direct numerical resolution of Eq. (4), even with $\epsilon = 1$, see Fig. 5.

Apart from the surprisingly good agreement (see discussion below), the new formula invites several comments. First, the stalling force is unaffected by the nonzero value

of ϵ. Indeed, one finds that stalling ($v = 0$) happens when $e^{-\mu} = \beta$ and in this case $\omega = \mu$, exactly. Hence, the condition for stalling remains $e^{-\omega} = \beta$, which is the usual formula in reduced notation. Second, when ϵ differs from zero, the new force-velocity relationship allows one to describe situations where the force on the obstacle is negative.

In order for a steady-state distribution to exist, one must have $\mu > 0$. The limit $\mu \to 0$ corresponds to the most negative force possible: $\omega_{\min} = -\epsilon(1-\beta)$, that is, dimensionally,

$$F_{\min} = -\frac{k_B T d}{D}(U_0 - W_0), \tag{77}$$

an exact formula valid for arbitrary ϵ. At that point, the velocity of the tip is given by the unimpeded value $v_{\max} = d(U_0 - W_0)$. For $F < F_{\min}$, the wall drifts away faster than the average bulk velocity of the tip and no stationary average distance x exists. Finally, in the case of zero applied force, Fig. 5 indicates a significant drop compared to $v_{\max}$, the value expected from the usual formula (2). Indeed, when $\epsilon = 0$, the diffusion time required to open an interval of length d is infinitely short compared to the chemical time. On the other hand, when $\epsilon > 0$, a finite time is necessary before the gap can open, which slows down the growth dynamics.

B. Time-dependent filament tip velocity

Above, we have used the steady-state distribution $c(x)$ to compute the expectation value of the polymer tip velocity. However, thanks to our analysis, we have access to the time-dependent distribution $c(x,t)$ and, hence, to the evolution of v:

$$v(t) = dU_0\left[\frac{\int_1^\infty c(x,t)dx}{\int_0^\infty c(x,t)dx} - \beta\right]. \tag{78}$$

In Appendix C, we evaluate the integrals above and find, after the fast, purely diffusive, transient and for $t > 1/\omega$,

$$v(t) \sim v_s(F)(1 + \epsilon\alpha e^{-\mu^2 t}), \tag{79}$$

where $v_s(F)$ is the stationary force-velocity relation computed in the preceding section and

$$\alpha = e^{\mu}\left(\frac{1-e^{-\mu}}{\mu}\right)^2. \tag{80}$$

Interestingly, the relaxation timescale appearing in Eq. (79) is completely distinct from t_ϵ, which we discovered in Sec. VI, even though it was obtained thanks to a perturbation expansion based on the smallness of ϵ. In fact, it coincides, up to $O(\epsilon)$ with t_s derived in Sec. IV. This difference of timescales can be explained as follows. While t_ϵ is the time required for the distribution to be fully affected by chemical effects, over a range $0 < x < 1/\epsilon$, one should recognize that most of the probability is concentrated within a range $0 < x < 3/\mu$. Therefore, expectation values of observable quantities such as v only require the transient to die out for values of x on the order of a few μ^{-1}. Using Eq. (50), we deduce that the duration of the transient for an observable quantity is not t_ϵ but rather $t \sim 1/(\mu\omega) \sim 1/\mu^2$.

C. Time-dependent filament wall velocity

Outside of steady state, the polymer tip and the wall do not necessarily move at the same speed. The expected value of the tip-wall distance

$$\langle x' \rangle = d\frac{\int_0^\infty xc(x,t)dx}{\int_0^\infty c(x,t)dx} \tag{81}$$

is not necessarily constant. The speed of the wall, which we denote by v_w, is thus related to the filament tip velocity by

$$v_w = v + \frac{d\langle x' \rangle}{dt'} = v + \frac{D}{d}\frac{d\langle x \rangle}{dt}. \tag{82}$$

In Appendix D, we find that

$$\frac{d\langle x \rangle}{dt} = \epsilon v \mu^2 t e^{-\mu^2 t}. \tag{83}$$

D. The reasons for the success of the ϵ expansion

The agreement found between the approximate and numerical solutions of Eq. (4) appears to be undeservedly good, given that ϵ is as large as as 1. Equation (72) explains the success of the above approximation procedure: For $x > n$, one has $h = 1 + O(\epsilon^{n+1})$, so that $c \sim \mu e^{-\mu x}$ with at least $O(\epsilon^{n+1})$ accuracy. Therefore, the accuracy of our approximation improves as x increases. Concerns about precision only arise for small values of x, and mostly in the range $0 < x < 1$, where slower convergence should be expected. However, if μ is sufficiently small, then most of the probability is distributed over large values of x [see Fig. 4(a)] so that the error for small x is weighted by a small probability. Specifically, the probability associated to the range $0 < x < 1$ is, in first approximation, $1 - e^{-\mu}$. In addition to that, Eq. (64) indicates that h_1 and, hence, all higher-order terms, are proportional to $1 - \beta e^{\mu}$, which is less than unity in the range $0 < \mu < \ln(1/\beta)$ provided, as usually assumed, that $\beta = W_0/U_0 < 1$. According to Eq. (75), this range corresponds to the positive values of v, with stalling arising precisely at $\mu = \ln(1/\beta)$. The range $0 < \mu < \ln(1/\beta)$ is thus the region of highest physical interest. While, for small μ, we have seen that our approximation scheme is naturally efficient, we further see that for larger value of μ, the approximation becomes more and more exact as $\mu \to \ln(1/\beta)$, since the corrections $\epsilon h_1, \epsilon^2 h_2, \ldots$ all tend to zero in that limit.

E. The large-μ, large-ω limit

To complete the above discussion, let us briefly examine the opposite limit of a large μ, which corresponds to a large nondimensional force ω. In that situation, and contrary to what has been examined before, all the probability is concentrated in the range $0 < x < 1$. Then, the equation for c is, approximately, in steady state,

$$c_{xx} + \omega c_x \approx -\epsilon[c(x+1) - \beta c(x)]. \tag{84}$$

Furthermore, in this last expression, we may neglect $c(x+1)$ in comparison to $c(x)$. We thus have, with very good approximation, regardless of ϵ,

$$c \sim \omega e^{-\omega x}[1 + O(\epsilon\beta/\omega)]. \tag{85}$$

Hence, for very large ω, the known formula (2) is recovered, as ϵ is effectively replaced by ϵ/ω.

F. Agreement with the exact formula when $\beta = 0$

In their paper, Peskin, Odell, and Oster were able to derive an exact formula, valid for any value of ϵ for the particular case $\beta = 0$:

$$v|_{\beta=0} = \frac{2D}{d}\frac{(\omega-\mu)\omega^2/2}{\omega^2 + (e^{\omega} - \omega - 1)\mu}. \tag{86}$$

Substituting, from Eq. (53), $\omega = \mu - \epsilon(1 - e^{-\mu})/\mu$, and expanding as $\epsilon \to 0$, one obtains

$$v \sim U_0 d e^{-\mu}\left\{1 + \frac{\epsilon}{\mu^2}[\mu - 2 + (2+\mu)e^{-\mu}]\right\}, \tag{87}$$

in agreement with the present theory.

IX. CONCLUSION

By revisiting the Peskin model for small but nonzero values of $\epsilon = U_0 d^2/D$, we were able to derive a number of new analytical results of practical interest. First, we identified the timescale t_s over which the fast, purely diffusive, transient takes place. This timescale approximately corresponds to the time required to dissipate an energy $k_B T$ by the wall friction in the absence of the polymer. The knowledge of this timescale is useful if one wishes to investigate a quasistatic limit where the applied force F varies slowly in time. Next, we showed how to apply the method of multiple scales to investigate the $O(\epsilon)$ chemical effects, including their transient. We showed analytically how the exponential distribution changes its rate, from ω to μ after a time t_ϵ, in very good agreement with direct numerical integration. In steady state, we showed how to obtain higher order approximations in a systematic way. A new parametrization, Eqs. (75) and (76) of the stationary force-velocity relationship was deduced, which again showed very good agreement with numerical integration, even when $\epsilon = O(1)$. As Fig. 5 illustrates, deviations from the previously known formula (for $\epsilon = 0$) can be significant. Finally, the relaxation of both the tip and the wall velocities toward their stationary value was derived. The timescale of this relaxation diverges as $\mu \to 0$, which corresponds to small applied forces.

From a methodological point of view, this paper showed how to apply the method of multiple scales to the one-filament Brownian ratchet equation. This method appears promising to address the multifilament problem; this will be the object of future research.

ACKNOWLEDGMENTS

G.K. is supported as a Research Associate of the Fonds De La Recherche Scientifique–FNRS (Belgium). We thank Marc Baus and Thomas Erneux for stimulating discussions.

APPENDIX A: RESOLUTION OF THE SHORT-TIME TRANSIENT

Here we give the details of the derivation of the solution (19). The drift term makes the problem given by Eq. (17) non-self-adjoint. We remove it by writing $c_0 = ue^{-\omega(x-x_0)/2 - \omega^2 t/4}$:

$$u_t = u_{xx}, \quad u(x,0) = \delta(x - x_0), \tag{A1}$$

with $u_x + \frac{\omega}{2}u = 0$ on $x = 0$. On the infinite line, the solution of the heat equation with a Dirac-δ initial condition would be $S(x - x_0, t)$, with

$$S(x,t) = \frac{e^{-x^2/4t}}{2\sqrt{\pi t}}. \tag{A2}$$

With the domain of definition of u restricted to positive values of x, we may write, more generally,

$$u = S(x - x_0, t) + \int_0^\infty S(x + s, t)\phi(s)ds, \tag{A3}$$

where $\phi(s)$ amounts to a suitably chosen distribution of point sources on the negative-x axis. With this ansatz, the boundary condition for u yields

$$0 = -S_x(x_0,t) + \frac{\omega}{2}S(x_0,t) + S(0,t)\phi(0) - \int_0^\infty S(s,t)\left[\phi'(s) - \frac{\omega}{2}\phi(s)\right]ds. \tag{A4}$$

For this condition to be satisfied at all times, one must have $\phi(0) = 0$ and

$$\phi'(x) - \frac{\omega}{2}\phi(x) = \delta'(x - x_0) + \frac{\omega}{2}\delta(x - x_0). \tag{A5}$$

The solution of this equation is

$$\phi(x) = \delta(x - x_0) + \omega e^{\omega(x-x_0)/2}H(x - x_0). \tag{A6}$$

Therefore

$$u = S(x - x_0, t) + S(x + x_0, t) + \omega\int_{x_0}^\infty e^{\omega(s-x_0)/2}S(x + s, t)ds. \tag{A7}$$

The integral above is $e^{-(x+x_0)\omega/2 + \omega^2 t/4}\frac{\omega}{2}\mathrm{erfc}(\frac{x+x_0-\omega t}{2\sqrt{t}})$. Equation (19) then follows directly.

APPENDIX B: EVOLUTION OF $C_1(X, \tau)$

The equation of evolution of $C_1(X, \tau)$ arises in a similar fashion as that of $C_0(X, \tau)$, namely as a solvability condition arising at $O(\epsilon^2)$. Omitting the detail, one finds unacceptable terms of the form $\epsilon^2 x e^{\omega x}$ unless

$$C_{1,\tau} + \omega C_{1,X} - (\beta - e^{-\omega} - \beta e^{\omega} + 1)C_1 = (e^{-\omega} - e^{\omega})C_{0,X} + C_{0,XX}. \tag{B1}$$

Note that the homogeneous part of the above equation is identical to Eq. (33). Hence any multiple of C_0 can be added to C_1. On the other hand, taking Eq. (46) into account, the right-hand side of the equation above yields a particular solution that is proportional, for $\tau > X/\omega$, to $XC_0(X, \tau)$. In other words, we now have secular divergence *on the slow spatial scale* X. To avoid this behavior, one simply needs to introduce a new, superslow scale,

$$\zeta = \epsilon^2 x, \tag{B2}$$

and require that, in fact,

$$C_0 = C_0(X, \zeta, \tau). \tag{B3}$$

Then Eq. (B1) becomes

$$C_{1,\tau} + \omega C_{1,X} + \omega C_{0,\zeta} - (\beta - e^{-\omega} - \beta e^{\omega} + 1)C_1 = (e^{-\omega} - e^{\omega})C_{0,X} + C_{0,XX} \tag{B4}$$

and the solvability condition on that equation is

$$\omega C_{0,\zeta} = (e^{-\omega} - e^{\omega})C_{0,X} + C_{0,XX}. \tag{B5}$$

This yields, for large-enough τ,

$$C_0 = e^{-(1-\beta e^{\omega})(1-e^{-\omega})X/\omega + \mu_2 \zeta}, \tag{B6}$$

where

$$\mu_2 = \frac{(1-\beta e^{\omega})(1-e^{-\omega})}{\omega^2} \times \left[e^{-\omega} - \beta e^{\omega} - \frac{1}{\omega}(1-\beta e^{\omega})(1-e^{-\omega}) \right]. \tag{B7}$$

This last expression is consistent with directly solving Eq. (53) up to $O(\epsilon^2)$ for μ in terms of ω. Once this superslow spatial dependence on C_0 is established, one finds that the equation for C_1 reduces to the equation for C_0 and hence that C_1 is a mere multiple of C_0. Such a reasoning carries over to any desired order.

APPENDIX C: TRANSIENT EXPECTED VALUE OF TIP VELOCITY

Combining the expressions derived in Secs. VI and VII,

$$c(x,t) \sim \mu e^{-\mu x} h(x) \begin{cases} 1 & x < \omega t \\ e^{\epsilon \nu (x - \mu t)} & x > \omega t \end{cases}, \tag{C1}$$

where ν is given by Eq. (58). Let us assume that $\omega t > 1$ and evaluate the expectation value of the polymer tip velocity:

$$\frac{v}{U_0 d} = \frac{\int_1^{\omega t} c dx + \int_{\omega t}^{\infty} c dx}{\int_0^1 c dx + \int_1^{\omega t} c dx + \int_{\omega t}^{\infty} c dx} - \beta. \tag{C2}$$

The various integrals above are

$$\int_0^1 c dx \sim 1 - e^{-\mu} - \frac{\epsilon}{\mu^2}[\mu - 2 + (\mu + 2)e^{-\mu}](1 - \beta e^{\mu}), \tag{C3}$$

$$\int_1^{\omega t} c dx \sim e^{-\mu} - e^{-\mu \omega t}, \tag{C4}$$

$$\int_{\omega t}^{\infty} c dx \sim \frac{\mu}{\omega} e^{-\epsilon \mu \nu t} e^{-\omega^2 t} \sim \left(1 + \frac{\epsilon \nu}{\mu}\right) e^{-\omega \mu t}, \tag{C5}$$

where we have used the fact that $\mu = \omega + \epsilon \nu$. Hence,

$$\int_1^{\infty} c dx \sim e^{-\mu} + \frac{\epsilon \nu}{\mu} e^{-\omega \mu t} \sim e^{-\mu} + \frac{\epsilon \nu}{\mu} e^{-\mu^2 t}, \tag{C6}$$

$$\int_0^{\infty} c dx \sim 1 - \frac{\epsilon}{\mu^2}[\mu - 2 + (\mu + 2)e^{-\mu}](1 - \beta e^{\mu}) + \frac{\epsilon \nu}{\mu} e^{-\mu^2 t}. \tag{C7}$$

Hence

$$\frac{v}{U_0 d} \sim (e^{-\mu} - \beta)\left\{1 + \frac{\epsilon}{\mu^2}[\mu - 2 + (2 + \mu)e^{-\mu}]\right\} + \epsilon \nu \frac{1 - e^{-\mu}}{\mu} e^{-\mu^2 t}. \tag{C8}$$

The last term can be expressed as

$$(e^{-\mu} - \beta)\epsilon e^{\mu} \left(\frac{1 - e^{-\mu}}{\mu}\right)^2 e^{-\mu^2 t}. \tag{C9}$$

APPENDIX D: EXPECTED VALUE OF THE TIP-WALL DISTANCE

Here we want to compute $d\langle x \rangle / dt$, where

$$\langle x \rangle = \frac{\int_0^{\infty} x c(x,t) dx}{\int_0^{\infty} c(x,t) dx}. \tag{D1}$$

The denominator is, using Eq. (C1)

$$\begin{aligned} \int_0^{\infty} x c dx &\sim \int_0^{\omega t} x c(x,t) dx + \int_{\omega t}^{\infty} x c(x,t) dx \\ &= \int_0^{\infty} \mu x e^{-\mu x} h(x) dx + \int_{\omega t}^{\infty} \mu x e^{-\mu x} h(x)[e^{\epsilon \nu (x - \mu t)} - 1] dx \\ &\sim \int_0^{\infty} \mu x e^{-\mu x} h(x) dx + \epsilon \nu \int_{\omega t}^{\infty} \mu x e^{-\mu x} h(x)(x - \mu t) dx, \end{aligned} \tag{D2}$$

where the expansion of the exponential in the last step is justified by the fact that the integrand is negligible when $\epsilon \nu (x - \mu t)$ ceases to be small. Hence,

$$\begin{aligned} \frac{d}{dt} \int_0^{\infty} x c dx &\sim \epsilon \nu [\mu x e^{-\mu x} h(x)(\mu t - x)]_{x = \omega t} \\ &\quad - \epsilon \mu \nu \int_{\omega t}^{\infty} \mu x e^{-\mu x} h(x) dx \sim -\epsilon \mu^2 \nu \\ &\quad \times \int_{\mu t}^{\infty} x e^{-\mu x} dx + O(\epsilon^2) \\ &= -\epsilon \nu (1 + \mu^2 t) e^{-\mu^2 t} + O(\epsilon^2). \end{aligned} \tag{D3}$$

On the other hand, with Eq. (C7),

$$-\frac{\int_0^{\infty} x c dx}{\left(\int_0^{\infty} c dx\right)^2} \frac{d}{dt} \int_0^{\infty} c dx \sim \epsilon \nu e^{-\mu^2 t}. \tag{D4}$$

Combining the two contributions,

$$\frac{d\langle x \rangle}{dt} \sim -\epsilon \nu \mu^2 t e^{-\mu^2 t}. \tag{D5}$$

[1] C. Peskin, G. Odell, and G. Oster, Biophys. J. **65**, 316 (1993).
[2] J. Howard, *Mechanics of Motor Proteins and the Cytoskeleton* (Sinauer, Sunderland, MA, 2001).
[3] T. L. Hill, Proc. Natl. Acad. Sci. USA **78**, 5613 (1981).
[4] L. Blanchoin, R. Boujemaa-Paterski, C. Sykes, and J. Plastino, Physiol. Rev. **94**, 235 (2014).
[5] E. Atilgan, D. Wirtz, and S. X. Sun, Biophys. J. **90**, 65 (2006).
[6] J. Weichsel and P. L. Geissler, PLoS Comput. Biol. **12**, e1004982 (2016).
[7] Y. Lan and G. A. Papoian, Biophys. J. **94**, 3839 (2008).
[8] D. Démoulin, M.-F. Carlier, J. Bibette, and J. Baudry, Proc. Natl. Acad. Sci. USA **111**, 17845 (2014).
[9] J. Condeelis, Annu. Rev. Cell Biol. **9**, 411 (1993).
[10] P. K. Mattila and P. Lappalainen, Nat. Rev. Mol. Cell Biol. **9**, 446 (2008).
[11] A. P. Liu, D. L. Richmond, L. Maibaum, S. Pronk, P. L. Geissler, and D. A. Fletcher, Nat. Phys. **4**, 789 (2008).
[12] I. Derényi, F. Jülicher, and J. Prost, Phys. Rev. Lett. **88**, 238101 (2002).
[13] M. J. Footer, J. W. J. Kerssemakers, J. A. Theriot, and M. Dogterom, Proc. Natl. Acad. Sci. USA **104**, 2181 (2007).
[14] A. Perilli, C. Pierleoni, G. Ciccotti, and J.-P. Ryckaert, J. Chem. Phys. **148**, 095101 (2018).
[15] A. Mogilner and G. Oster, Biophys. J. **71**, 3030 (1996).
[16] N. J. Burroughs and D. Marenduzzo, J. Phys.: Condens. Matter **18**, S357 (2006).
[17] A. Perilli, C. Pierleoni, and J.-P. Ryckaert, J. Chem. Phys. **150**, 185101 (2019).
[18] C. Pierleoni, G. Ciccotti, and J.-P. Ryckaert, J. Chem. Phys. **143**, 145101 (2015).
[19] R. Wang and A. E. Carlsson, New J. Phys. **16**, 113047 (2014).
[20] F. Motahari and A. E. Carlsson, arXiv:1812.00061v1.
[21] U. Dobramysl, G. A. Papoian, and R. Erban, Biophys. J. **110**, 2066 (2016).
[22] K. Tsekouras, D. Lacoste, K. Mallick, and J.-F. Joanny, New J. Phys. **13**, 103032 (2011).
[23] J. Ockendon, S. Howison, A. Lacey, and A. Movchan, *Applied Partial Differential Equations* (Oxford University Press, Oxford, 2003).
[24] See Supplemental Material at http://link.aps.org/supplemental/10.1103/PhysRevE.100.022132 for MATHEMATICA and MATLAB files.
[25] H. Wang, C. Peskin, and T. C. Elston, J. Theor. Biol. **221**, 491 (2003).